Steady-State Theory of Current Transfer

Vered Ben-Moshe and Abraham Nitzan*

School of Chemistry, Tel Aviv University, Tel Aviv 69978, Israel

Spiros S. Skourtis

Department of Physics, University of Cyprus, Nicosia 1678, Cyprus

David N. Beratan

Department of Chemistry, Duke University, Durham, North Carolina 27708

Received: January 23, 2010; Revised Manuscript Received: March 7, 2010

Current transfer is defined as a charge-transfer process where the transferred charge carries information about its original motion. We have recently suggested that such transfer causes the asymmetry observed in electron transfer induced by circularly polarized light through helical wires. This paper presents the steady-state theory of current transfer within a tight binding model of coupled wires systems. The asymmetry in the system response to a steady current imposed in a particular direction on one of the wires is used to define the efficiency of current transfer.

1. Introduction

Current transfer is defined as the transfer of a charge carrier while preserving characteristics of its momentum. In a recent paper,[1] we presented a tight-binding charge transfer model for experimental observations[2,3] that indicate that photoelectron transfer induced by circularly polarized light through helical molecular bridges depends on the relative handedness of the bridge helicity and on the optical circular polarization. Another recent example of current transfer in photoemission is provided by ref 4, where the signature of a biased linear momentum distribution created on a Cu (100) surface is observed in the angular distribution of the photoemitted current. Our rationalization of the experimental results of refs 2, 3 was based on the assumption that excitation by circularly polarized light can create a circular electronic current in the absorbing molecule or surface (this assumption is supported by theoretical analysis[5−8]), and that chirality may control the transmission of these currents as a consequence of atoms' proximity. Figure 1 illustrates this idea.

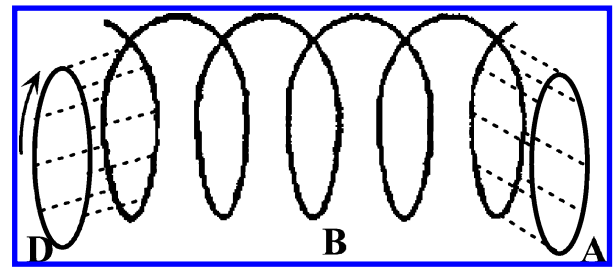

Figure 1. Circular current in the donor (D) ring is transferred to an acceptor A through a helical bridge. The dominant intermolecular coupling, illustrated by dotted lines connecting nearest atoms belonging to neighboring molecules can coherently transmit directional information. The clockwise circular current indicated by the arrow on the donor will be transmitted through the helical bridge shown more readily than a circular current in the opposite direction.

Figure 1 shows how the current transfer phenomenon may originate from the coupling scheme, which results here from proximity of circular/helical molecular structures, and the preparation of the donor state. Other molecular structures that may show the same physical behavior are displayed in Figure 2. Figure 2a represents an electron transmission structure studied by Lin et al.,[9] in which a noncovalent contact bridges between oligo(phenylene ethynylene) units. Figure 2b shows a designed $\pi-\sigma-\pi$ motif with a saturated spirocyclic linkage between oligothiophenes chains that was suggested by Aviram[10] as a possible component in a molecular memory device. In this structure, the spirocyclic linkage inserts 4 σ bonds between the unsaturated chains. Both systems could enable current transfer to be observed if current were driven in one of the linked chains and the induced current were monitored in the other chain.

Figure 3 shows simple theoretical models for current transfer. Each model corresponds to a tight-binding Hamiltonian with nearest-neighbor couplings indicated by the bonds connecting different sites. In the model in Figure 3a, we consider a wire D (the "driver") carrying a current J_D and investigate the possibility of current transfer to wire A through a coupling region defined by coupling matrix elements V_{ij} between N_{DA} pairs of neighboring atoms i and j on different wires. This coupling will appear in the system Hamiltonian written in the site representation. In Figure 3a, where $N_{DA} = 3$, this coupling region includes atoms 1, 2, and 3 on wire D; 5, 6, and 7 on A; and the couplings $V_{1,5}$, $V_{2,6}$, and $V_{3,7}$ between them. Any charge transferred from D to A will flow to the right of site 7 and to the left of site 5. We denote these currents J_{AR} and J_{AL}, respectively. A signature of current transfer may be taken as $J_{AR} \neq J_{AL}$ or, in the case of a transient (pulse) current, $\int_{-\infty}^{\infty} dt\ J_{AR}(t) \neq \int_{-\infty}^{\infty} dt\ J_{AL}(t)$; the integrals expressing the total charge transferred rightwards and leftwards through wire A. The model in Figure 3b is similar, except that the transfer D → A is mediated through a bridging wire B. Here N_{DB}, N_{BA}, and N_B (2, 2, and 1 in this example) denote respectively the number of site pairs connecting the wires D and B, the corresponding number between wires B and A, and the number of B sites between these coupling regions. In the case represented by Figure 3b, the signature of current transfer is similar, except that J_{AR} and J_{AL} now express charge

10.1021/jp100661f
Published on Web 04/13/2010

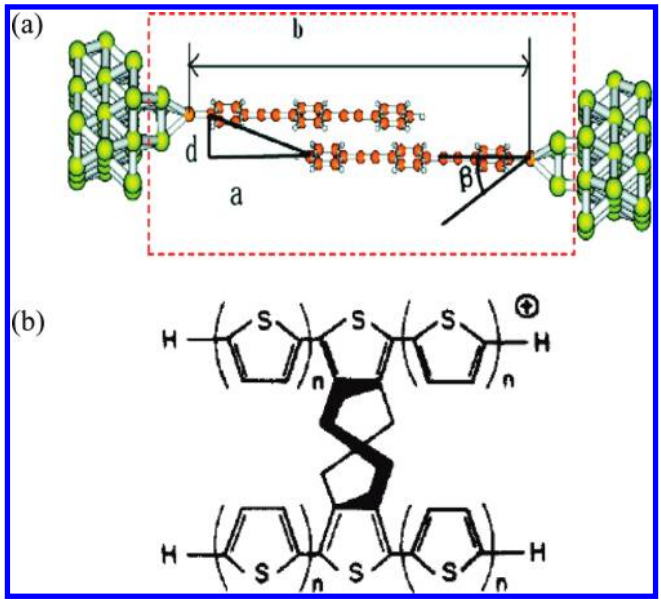

Figure 2. (a) Through-space linked oligo(phenylene ethynylene) structures.[9] (b) Saturated spirocyclopentane linked thiophenes.[10] In both cases, the effective electronic interaction across the chain-to-chain contacts is estimated to be about 100-fold weaker than the nearest-neighbor interactions within the chains.

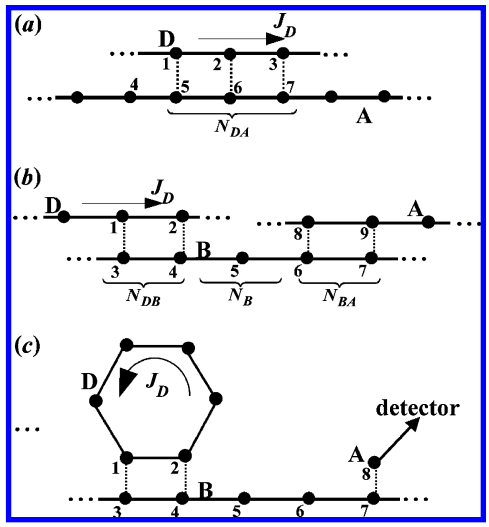

Figure 3. Simple models of current transfer. In these models a current in wire D is transferred to wire A. In (a) the transfer is direct while in (b) it is mediated by a "bridge" wire B. Model (c) is a variant of (b), where the driving current J_D arises from a circular current on the donor ring D. The arrow represents an irreversible transition out of A.

transfer rates through the "acceptor" A for a rightward or leftward going driving current J_D. The model of Figure 3c is a version of the model in Figure 3b, in which the driving current originates from a circular current on the donor (D) ring. In particular, the current direction between sites 1 and 2 that couple to the rest of the system reflects the circular polarization of the ring current. Also in Figure 3c, we emphasize that the nature of the accepting system A is not very important in this case. The only requirement is that some signal proportional to the population in A is induced in the detector. The signature of current transfer is then an asymmetry in this signal under direction reversal of the driving current. Note that current transfer as defined here arises in these tight-binding models only if the driver wire D is coupled to the wires A in Figure 3a or B in Figures 3b,c by more than a single interaction. Indeed, the directional information associated with the transfer is conveyed through interference among different transfer paths. This implies that thermal interactions and dephasing processes may have strong effects on current transfer processes.

In ref 1, we described a time dependent approach to current transfer, where a transient current J_D is initially generated by a pulse excitation. There are situations, e.g., those pertaining to molecular conduction phenomena, where the complementary steady-state description is advantageous. The present paper presents the steady-state approach to this problem. Here we obtain the steady-state of the system when driven by a constant current on wire D and evaluate the currents induced in other parts of the system subject to this driving. The current transfer efficiency may be quantified by the asymmetry factor

$$\mathcal{A} = \frac{J_{AR} - J_{AL}}{J_{AR} + J_{AL}} \tag{1}$$

that measures the transfer of directionality information from the driving current. Our objective is to examine the dependence of this asymmetry on the molecular structure expressed by the coupling scheme, the intrachain and interchain site energies and the coupling strengths and the dephasing caused by thermal interactions.

2. Model Hamiltonian and the Steady-State Analysis

For definiteness, we focus on the model of Figure 3b, which describes the driving wire D, the bridging wire B and the accepting wire A as linear tight-binding chains. The corresponding Hamiltonian is $\hat{H} = \hat{H}_D + \hat{H}_A + \hat{H}_B + \hat{V}_{BA} + \hat{V}_{BD}$, where

$$H_K = \sum_{j_K \in K} E_{j_K}^{(K)} |j_K\rangle\langle j_K| + \sum_{j_K \in K} V_{j_K j_K+1}^{(K)} |j_K\rangle\langle j_K + 1| + \text{h.c.} \qquad K = \text{D, A, B} \tag{2}$$

and

$$V_{K,K'} = \sum_{j_K \in K,} \sum_{j_{K'} \in K'} V_{j_K j_{K'}}^{K,K'} |j_K\rangle\langle j_{K'}|; \quad (K, K') = (\text{D, B}) \quad \text{or} \quad (\text{B, A}) \tag{3}$$

Here $\hat{H}_D$, $\hat{H}_B$, and $\hat{H}_A$ are the Hamiltonians for the D, B, and A moieties, respectively, and $\hat{V}^{(DB)}$ ($\hat{V}^{(BA)}$) are the D−B (A−B) interactions. When the driving wire is an N_D-member cyclic molecule as in Figure 3c, this cyclic periodicity is reflected by the additional condition $\Psi(j_D + N_D) = \Psi(j_D)$. The values of the interchain coupling elements $V_{j_K j_{K'}}^{(K,K')}$ in eq 3 reflect the geometry of the molecular structures, e.g., the proximity of atoms belonging to different molecules. Here too we assume nonzero coupling only between sites on different wires that are nearest to each other, e.g, the site pairs (1,5), (2,6), and (3,7) in Figure 3a or (1,3) and (2,4) in Figure 3, panels b and c. Below, we consider the specific case where each wire is a sequence of similar sites and all intersite couplings are the same for similar pairs of sites. Accordingly, we denote

$$\alpha_K = E_{j_K}^{(K)}; \quad \beta_K = V_{j_K j_K+1}^{(K)}; \quad V_{KK'} = V_{j_K j_{K'}}^{(K,K')} \tag{4}$$

In ref 1, we studied the time evolution that follows the excitation of ring current in the driving wire (e.g., Figure 3c). If the ring has N_D equivalent sites this initial state is described by the Bloch wave function

$$\Psi(t = 0) = \sqrt{\frac{a}{L}} \sum_{j_D=1}^{N_D} e^{i(j_D-1)ka} |j_D\rangle \tag{5a}$$

with

$$k = \frac{2\pi M}{aN_D}; \quad M = 0, \pm 1, ..., \pm N_D - 1; \quad L = N_D a \tag{5b}$$

where α is the intersite distance. Here, the driving wire is restricted to remain in this state, and we require the steady state assumed by the rest of the system under this restriction. The most relevant sites on the driver are those that are directly coupled to wire B, e.g., sites 1 and 2 in Figure 3b,c. The driving restriction in this case is

$$\psi_D(t) = c_1(t)|1\rangle + c_2(t)|2\rangle = (\bar{c}_1|1\rangle + \bar{c}_2|2\rangle)\, e^{-(i/\hbar)E(k)t} \tag{6a}$$

$$\bar{c}_2 = \bar{c}_1 e^{ika} \tag{6b}$$

where E and k are related by the characteristic 1−d tight binding dispersion relation

$$E(k) = \alpha_K + 2\beta_K \cos(ka) \quad (\text{here } K = D) \tag{7}$$

Note that in steady-state situations the injection energy is not determined by the energy of a donor or acceptor state. The steady state essentially describes a scattering process at an energy (or energy regime) determined by the driving process.

For the system to reach steady state, the acceptor wire A must be infinite, as in Figure 3b. Alternatively, the population in the acceptor site A must be assumed to be depleted by coupling to an external sink as in Figure 3c. This depletion is not part of the Hamiltonian of eqs 2 and 3 and must be added as phenomenological terms in the time dependent Schrödinger equation. In either case, the ensuing currents in the acceptor are the detected outcome of the driving process.

For the model Hamiltonian of eqs 2 and 3 the time-dependent Schrödinger equation in the site representation is

$$\hbar \frac{dc_n}{dt} = -iE_n c_n - i\sum_\alpha V_{n,\alpha} c_\alpha \tag{8}$$

where α sums over all sites that couple (with coupling elements $V_{n,\alpha}$) to site n. At steady state, driven as described by eq 6a (or its equivalent for the system of Figure 3a), we expect a solution of the form

$$c_n(t) = \bar{c}_n e^{-iEt/\hbar} \tag{9}$$

Using 9 in 8 gives

$$0 = -i(E_n - E)\bar{c}_n - i\sum_\alpha V_{n,\alpha}\bar{c}_\alpha \tag{10}$$

Equations 10 are linear algebraic equations for the coefficients $\{\bar{c}_n, n \in B,A\}$ that define the steady-state wave function, $\Psi(t) = \sum_{n\in B,A} c_n(t)|n\rangle$, on the B and A wires. Terms involving $\{\bar{c}_n, n \in D\}$ appear as inhomogeneous source terms in these equations.

The driving current on the D wire provides a source of charge carriers in the system. For eq 8 to yield the steady-state form at long time, eqs 9 and 10, it has to be supplemented by terms describing population absorption. In ref 1, this was achieved by assigning (real and positive) decay rates γ_j to some sites by replacing E_j by $E_j - ((1/2)\gamma_j)$ for these sites in eqs 8 and 10. The outgoing rate from the acceptor site A in Figure 3c may be described in this way. In the present case, the infinite extent of the B and A wires of Figures 3 provide effective sinks for damping population in the relevant (observed) part of the system that can be represented rigorously. Indeed, eqs 8 and 10 represent an infinite set of equations that can be made finite by the usual technique of separating the overall system into an interior "relevant" part and a remaining exterior part, and accounting for the effect of the latter on the dynamics of the former using an appropriate "self-energy" term. In particular, in Figure 3a, the effect of an exterior part defined as the infinite linear chain extending beyond the cutoff site 7 on A is manifested by modifying eq 10 for this site according to

$$0 = -i(E_A + \Sigma_A(E) - E)\bar{c}_7 - i\beta_A\bar{c}_6 - iV_{AD}\bar{c}_3 \tag{11}$$

$\Sigma_A(E)$ is the self-energy of a 1-dimensional tight-binding wire, with real and imaginary parts $\Lambda_A(E)$ and $-i(\Gamma_A(E)/2)$, respectively

$$\Sigma_K(E) = \frac{E - E_K - \sqrt{(E - E_K)^2 - 4\beta_K{}^2}}{2} \equiv \Lambda_K(E) - \frac{i}{2}\Gamma_K(E) \qquad K = B, A \tag{12}$$

A full finite set of steady-state equations, for example, the model in Figure 3b may be written as

$$\begin{aligned}
0 &= -i(E_B + \Sigma_B(E) - E)\bar{c}_3 - i\beta_B\bar{c}_4 - iV_{BD}\bar{c}_1\\
0 &= -i(E_B - E)\bar{c}_4 - i\beta_B\bar{c}_3 - i\beta_B\bar{c}_5 - iV_{BD}\bar{c}_2\\
0 &= -i(E_B - E)\bar{c}_5 - i\beta_B\bar{c}_4 - i\beta_B\bar{c}_6\\
0 &= -i(E_B - E)\bar{c}_6 - i\beta_B\bar{c}_5 - i\beta_B\bar{c}_7 - iV_{BA}\bar{c}_8\\
0 &= -i(E_B + \Sigma_B(E) - E)\bar{c}_7 - i\beta_B\bar{c}_6 - iV_{BA}\bar{c}_9\\
0 &= -i(E_A + \Sigma_A(E) - E)\bar{c}_8 - i\beta_A\bar{c}_9 - iV_{AB}\bar{c}_6\\
0 &= -i(E_A + \Sigma_A(E) - E)\bar{c}_9 - i\beta_A\bar{c}_8 - iV_{AB}\bar{c}_7
\end{aligned} \tag{13}$$

or

$$\mathbf{Mc} = \mathbf{d} \tag{14}$$

where $\mathbf{c}$ is the column vector trans($\bar{c}_3$,$\bar{c}_4$,$\bar{c}_5$,$\bar{c}_6$,$\bar{c}_7$,$\bar{c}_8$,$\bar{c}_9$), $\mathbf{M}$ is the matrix multiplying this vector in eq 13, and $\mathbf{d}$ is the driving vector trans($iV_{BD}\bar{c}_1$,$iV_{BD}\bar{c}_2$,0,0,0,0,0) ("trans" denotes the transpose). Note that in the phenomenological approach discussed above and in ref 1, $\Sigma_K(E)$, K = B,A, are replaced by constant damping terms $-(1/2)i\gamma_j$ (for site j) representing couplings to some arbitrary broad-band dissipation channels. Using the self-energies associated with infinite 1-dimensional chains has the advantage of providing reflectionless interfaces, making it easier to identify and quantify current transfer processes in steady-state situations.

Inverting eq 14 and using eq 6b yields all coefficients in terms of $\bar{c}_1$. This makes it possible to evaluate all currents in the system in terms of the driving current on wire D as described in the next section.

3. Steady-State Currents and Current Asymmetry Factors

Using eqs 8−10 with E_n replaced by $E_n + \Sigma_n(E)$ when n is an edge site produces the steady state (SS) equation for the population on site n

$$0 = \left(\frac{d|c_n(t)|^2}{dt}\right)_{SS} = \sum_\alpha \frac{2V_{n,\alpha}}{\hbar} Im(c_\alpha c_n^*) - \frac{\Gamma_n(E)}{\hbar}|c_n|^2\delta_{n,\text{edge}} \tag{15}$$

where, as in eq 8, the sum runs over all sites that couple to site n with coupling elements $V_{n,\alpha}$ ($V_{n,\alpha} = \beta_K$ if both n and α belong to wire K; $V_{n,\alpha} = V_{K,K'}$ if these sites are nearest neighbors belonging to different wires K and K'). The term containing

$\Gamma_n(E) = -2Im\ \Sigma_n(E)$ contributes only if site n is an edge site on the bridge ($\Gamma_n = \Gamma_B$), or on the acceptor wire ($\Gamma_n = \Gamma_A$).

Equation 15 is a continuity law that describes conservation of probability; it can be used to identify the current between any two sites as well as the current entering and leaving a given system. In particular, eq 15 implies that the current from site $n-1$ to site n on a given wire K is

$$J_{K(n-1\rightarrow n)} = \frac{2\beta_K}{\hbar} Im(c_{n-1}c_n^*) \tag{16}$$

and the current out of the system at the edge site n on wire K is

$$J_{K(n\rightarrow \text{out})} = \frac{\Gamma_n(E)}{\hbar}|c_n|^2 \tag{17}$$

In the following analysis, unless otherwise stated, we assign positive signs to currents from left to right, from D to B, from D to A, and from B to A.

It is useful to consider the application of eqs 16 and 17 to the special case of current on a linear tight-binding chain. With $c_n = c_{n-1}e^{ika}$, we find

$$J_{K(n-1\rightarrow n)} = -\frac{2\beta_K}{\hbar}|c_n|^2 \sin(ka) \tag{18}$$

[Near the bottom of the band, $k \rightarrow 0$ (see eq 7) and $J_{K(n-1\rightarrow n)} = -(2\beta_K/\hbar)|c_n|^2 ka$. The fact that for positive k a positive (left to right) current is associated with negative β_K is related to the fact that the kinetic energy operator on a grid of spacing h is given by $-f''(x) \approx -h^{-2}[f(x+h) - 2f(x) + f(x-h)]$.] For a current in the direction $n-1 \rightarrow n \rightarrow$ out, eq 16 indicates that $\beta_K \sin(ka)$ needs to be negative. Current conservation implies that

$$\Gamma_K(E) = 2|\beta_K \sin(ka)| \tag{19}$$

and using (cf. eq 7) $\cos(ka) = (E - \alpha_K)/2\beta_K$ gives

$$\Gamma_K(E) = 2|\beta_K|\sqrt{1 - \left(\frac{E-\alpha_K}{2\beta_K}\right)^2} \tag{20}$$

which is consistent with eq 12. Furthermore, eqs 7 and 12 imply

$$\Lambda_K(E) = \beta_K \cos(ka) = \frac{E-\alpha_K}{2} \tag{21}$$

Equations 20 and 21 hold for E inside the K-wire energy band.

We now consider the steady-state currents induced in the system by a driving current on the D wire, defined by eqs 6a and 7 with $k = k_D$ and $E = E(|k_D|)$. In particular, for the DA model of Figure 3a, we focus on the current out of the A wire to the right and to the left. It is convenient to define both currents as positive quantities

$$J_A^{\text{right}} = \frac{2\beta_A}{\hbar} Im(c_{\text{eright}-1}c_{\text{eright}}^*) = \frac{\Gamma_A(E)}{\hbar}|c_{\text{eright}}|^2 \tag{22}$$

$$J_A^{\text{left}} = \frac{2\beta_A}{\hbar} Im(c_{\text{eleft}+1}c_{\text{eleft}}^*) = \frac{\Gamma_A(E)}{\hbar}|c_{\text{eleft}}|^2 \tag{23}$$

where eright and eleft denote the right and left edge sites on the A wire, respectively. Symmetry requires that $J[\text{right,A},k_D] = J[\text{left,A},-k_D]$. A nonzero current asymmetry factor

$$\mathcal{A}_1 = \frac{J_A^{\text{left}} - J_A^{\text{right}}}{J_A^{\text{left}} + J_A^{\text{right}}} \tag{24}$$

is a signature of current transfer; that is, it indicates that a signature of momentum, i.e., directional information, is transferred together with the charge.

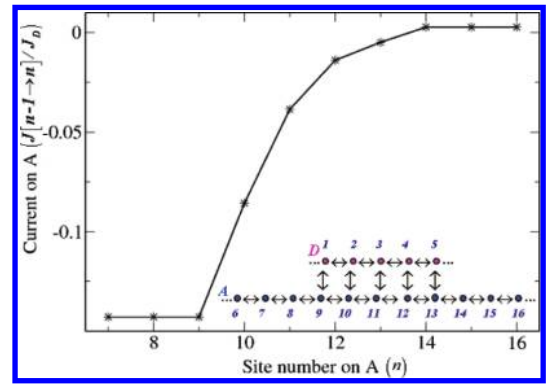

Figure 4. Current distribution on wire A of the DA system shown in the inset, characterized by 5-site coupling between the D and A wires. Parameters are $|J_D| = 1$, $E_D = E_A = 0$, $\beta_D = \beta_A = 0.1$, $V_{DA} = 0.01$ and the injection energy is $E = -0.15$. The phase $k_D a = \arccos[(E - E_D)/2\beta_D]$ is taken positive, implying that the driving current is leftward.

We now consider similar asymmetry factors for the B and A wires in the DBA model of Figure 3b. A better measure of current transfer in this case is the dependence of the total current, J_A^{total}, transmitted to the A wire on the direction of the driving current on the D wire, characterized by the asymmetry factor

$$\mathcal{A}_2 = \frac{J_A^{\text{total}}(-k_D) - J_A^{\text{total}}(k_D)}{J_A^{\text{total}}(-k_D) + J_A^{\text{total}}(k_D)} \tag{25}$$

$\mathcal{A}_2$ is directly related to the observations in refs 2 and 3, and it quantifies the effect of the current-transfer information mediated through the bridge B on the D $\rightarrow$ A charge transfer. This asymmetry can be studied as a function of the energy level positioning of wire B relative to the D and A wires, and as a function of the B-wire length. Measures of different normalization are also useful

$$\tilde{\mathcal{A}}_1 = \frac{J_A^{\text{left}} - J_A^{\text{right}}}{|J_D|} \tag{26}$$

$$\tilde{\mathcal{A}}_2 \equiv \frac{J_A^{\text{total}}(-k_D) - J_A^{\text{total}}(k_D)}{|J_D|} \tag{27}$$

where J_D is the donor (driving) current.

Figure 4 shows the current distribution in the A wire of the DA system illustrated in the inset. Here and below, all energy units are relative; and the reader may assign them as convenient, e.g., take all of the numbers given for energies in electron volts. The driving current induces left and right going currents at the left and right sides, respectively, of the A wire. The current is position independent in all parts of A that are not coupled to the driving wire, and changes in the coupling region. The larger leftward current on A reflects the directionality transfer, i.e. the current transfer character of the process. This asymmetry, and its counterpart in the DBA system are expressed in the figures below using the current asymmetry factors $\mathcal{A}_1$ and $\mathcal{A}_2$.

We next show numerical results for these asymmetry factors that indicate their dependence on system parameters and structure. The structure is expressed in terms of the number of links (coupled site-pairs), N_{DA}, connecting the D and A wires in the DA system, the corresponding numbers N_{DB} and N_{BA} in the DBA system and the length N_B of the bridge segment separating the DB and BA coupling regions in the DBA system (see Figure 5). For the structure displayed in Figure 1, N_{DA} and N_{DB} are the number of dashed lines connecting the ring to the helical bridge on the left and right, respectively, while N_B

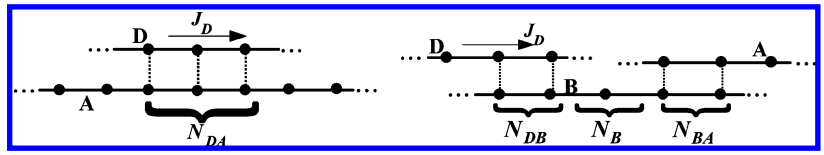

Figure 5. Structural parameters in the DA and DBA systems. N_{DA}, N_{DB}, and N_{BA} are the number of links connecting the wires D, B, and A. N_B is the length of the bridge segment between the D−B and the B−A coupling regions in the DBA system.

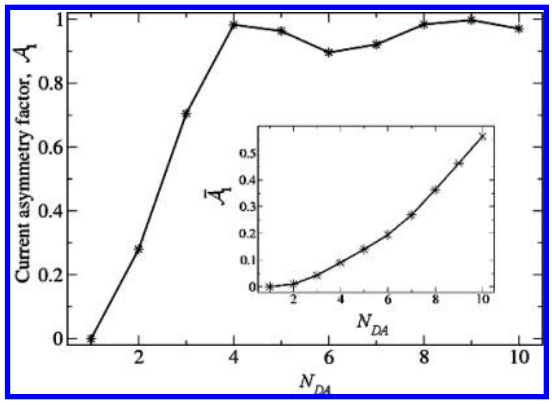

Figure 6. Current asymmetry factor $\mathcal{A}_1$ as a function of the number of links (N_{DA}) connecting the D and A wires in the DA system (Figure 5). The inset shows the same data, presented in terms of $\bar{\mathcal{A}}_1$ vs N_{DA}. Parameters are the same as in Figure 4.

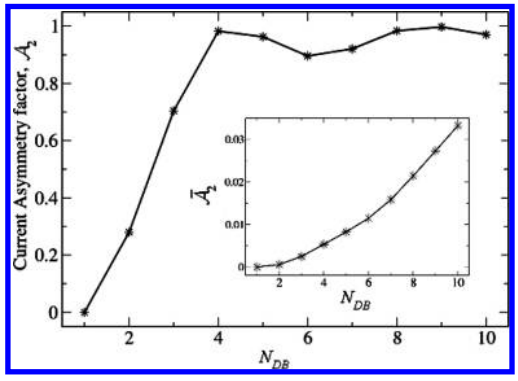

Figure 7. Current asymmetry factor $\mathcal{A}_2$ displayed vs the number of links N_{DB} connecting the D and B wires in the DBA system of Figure 5. Parameters are similar to Figure 4: $E_D = E_B = E_A = 0$; $\beta_D = \beta_B = \beta_A = 0.1$, $V_{DB} = V_{BA} = 0.01$, $N_{BA} = 1$ and the injection energy $E = -0.15$. The inset shows the same data, presented as $\bar{\mathcal{A}}_2$ vs N_{DB}.

corresponds to the length of the helical bridge. Another characteristic parameter is the ratio V/β between the interchain and intrachain coupling parameters. In the systems shown in Figure 2, the tunneling gap is ~3.5 Å for Figure 2a, and ~5 Å for Figure 2b. Assuming a typical through sigma-bond decay parameter of 0.6,[11] and a through-space distance decay exponent of 1.1 Å^{-1} (computed for an electron binding energy of ~5 eV), the tunneling amplitude attenuation across both interfaces is expected to be $\sim 10^{-2}$. In the simple models of Figures 3 and 5 this would imply $V_{DA} \sim 10^{-2} \times \beta$. We have found that the calculated asymmetry factors $\mathcal{A}_1$ and $\mathcal{A}_2$ are not sensitive to V_{DA}/β although the absolute current in the A wire and consequently the asymmetry factors $\bar{\mathcal{A}}_1$ and $\bar{\mathcal{A}}_2$ are sensitive to this ratio.

Figure 6 shows the current asymmetry factor $\mathcal{A}_1$ for the DA system of Figure 5 as a function of the number of links (coupled site-pairs), N_{DA}, connecting the D and A wires ($\mathcal{A}_1 = 0$ for $N_{DA} = 1$). Figure 7 shows the corresponding $\mathcal{A}_2$ value for the DBA system of Figure 5. In both cases, asymmetry increases and then saturates near 1 (when the response current becomes nearly unidirectional) as N_{DA} increases.

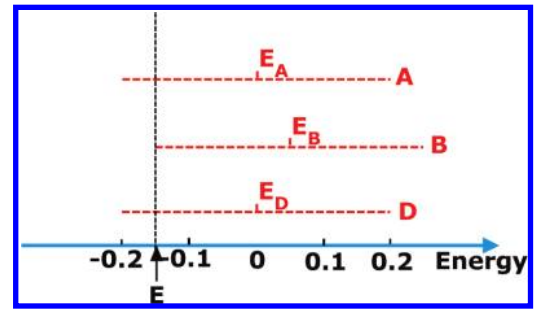

Figure 8. Schematic illustration of the band structures in the three wire DBA system. The horizontal (red) dashed lines correspond to the bands of the D, B, and A wires as indicated. E is the injection energy (here −0.15) which, in the example shown, coincides with lower band edge of the B wire.

The large asymmetries in the above results indicate the substantial current transfer character that may arise for both the direct transfer (the DA model) and the bridge assisted process (the DBA model). The infinite bridge length is particularly important in this steady-state process. For a short bridge, the selective directionality underlying the current transfer may be diminished or eliminated by wave function reflection at the edge of the B wire. In this respect, the steady-state situation is different from the transient process described in ref 1, where, for short pulses, reflection does not set in appreciably during the time-scale of the process.

Another important factor discussed in ref 1 is the energy dependence of the current transfer, namely the resonant or nonrsonant nature of the process. The results in Figures 4, 6, and 7 correspond to resonance transmission, where site energies in all wires are equal. Superexchange-mediated current transfer may arise in DBA systems where the bridge energy E_B is different from the site energies $E_D = E_A$ of the "donor" and "acceptor" wires. Because of the finite bandwidths, the onset of the superexchange mechanism depends on the band structure of the wires and on the injection energy E. In the calculation below, we take $E_D = E_A = 0$, $\beta_D = \beta_A = \beta_B = 0.1$, and an injection energy $E = -0.15$, and vary the bridge energy E_B. Since energy bands in these tight-binding wires are in the range $E_K \pm 2\beta_K$ (K = D, B, A), nonresonant transfer occurs when $E_B > 0.05$ or $E_B < -0.35$ (Figure 8). Figure 9 shows the current transfer behavior for this system in the off-resonance regime, $E_B > 0.05$. We find a strong exponential damping of the current transfer property expressed by the asymmetry factor $\mathcal{A}_2$. It should be emphasized that, as defined, the behavior of $\mathcal{A}_2$ reflects the erasure of the current transfer, i.e., the momentum transfer property and not the damping of the charge transfer itself.

Figure 9 shows that the current transfer property decays quickly as transport enters the off-resonance (superexchange) transfer regime. One might expect that a similar drop in asymmetry will also be seen as we approach the edge of the resonance transfer regime from the resonance side, e.g., $-0.35 < E_B < 0.05$ for the parameters used in Figure 9. Figure 10 shows that the behavior approaching the band edges from within the band is more complicated, although $\mathcal{A}_2$ indeed goes smoothly

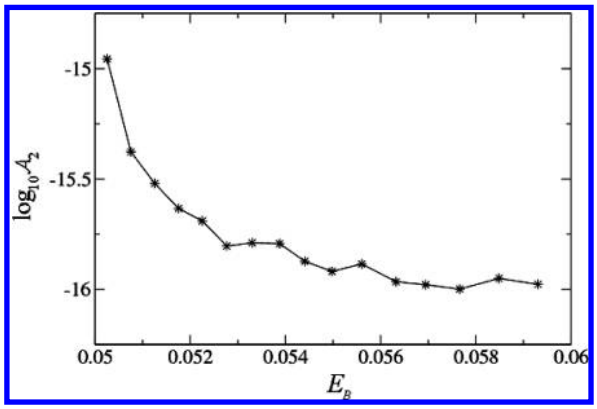

Figure 9. Current asymmetry factor $\mathcal{A}_2$ vs bridge site energy E_B for the DBA system in the off-resonance (superexchange) regime for $E_D = E_A = 0$, $\beta_D = \beta_B = \beta_A = 0.1$, $V_{DB} = V_{BA} = 0.01$, $E = -0.15$, $N_{DB} = 2$, $N_B = 1$, $N_{BA} = 1$. Shown is the current transfer behavior of the system in the superexchange regime, $E_B > 0.05$. Coarse-grained averaging was applied to reduce numerical errors that result from computing small differences among relatively large numbers.

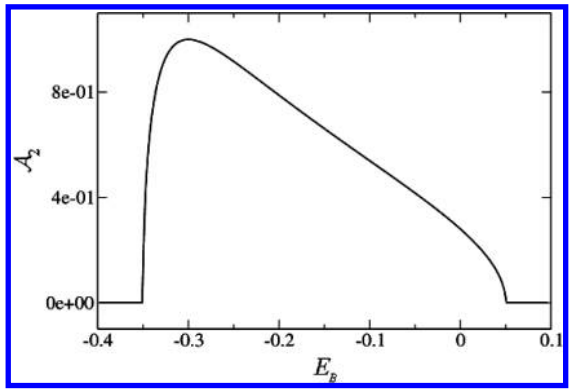

Figure 10. Current asymmetry factor $\mathcal{A}_2$ vs the site energy E_B of the B wire in the DBA system. Parameters are the same as in Figure 9.

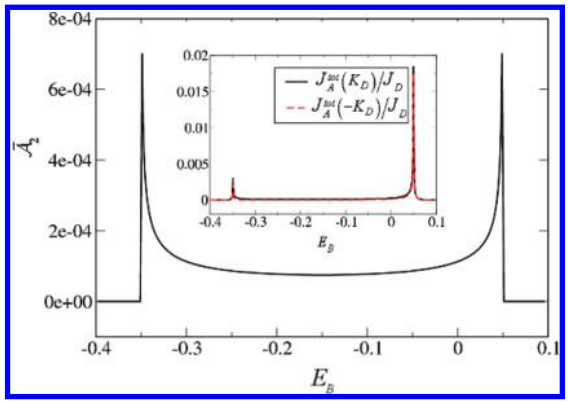

Figure 11. Same data as in Figure 10, now represented in terms of $\bar{\mathcal{A}}_2$, eq 27, shown vs E_B in the resonance transmission regime. Parameters are the same as in Figure 9. The inset shows the individual contributions, $J_A^{total}(\pm k_D)/J_D$.

to a very small value as we approach the band edge. It is notable that the charge transfer itself, expressed by the absolute current in the A wire, is singular at the band edge. This is seen in Figure 11 which shows $\bar{\mathcal{A}}_2$ in analogy with Figure 10. Similar behavior is obtained for the individual components, $J_A^{total}(\pm k_D)/J_D$ of $\bar{\mathcal{A}}_2$), shown in the inset. Remarkably, the individual right and left currents on wire A can be larger than the driving current J_D.

The origin of the band-edge singularities seen in Figure 11 are explained by considering the simpler model shown in Figure 12 (left). Here, a single link connects the D and A wires, and directionality information cannot be transferred. Indeed, the only property of the D wire that affects the A wire is the amplitude oscillation at site 2 determined by the injection energy E, $c_2(t) = \bar{c}_2 e^{-(i/\hbar)Et}$. At steady state, the amplitude $c_3(t)$ behaves similarly, $c_3(t) = \bar{c}_3 e^{-(i/\hbar)Et}$, where $\bar{c}_3$ satisfies

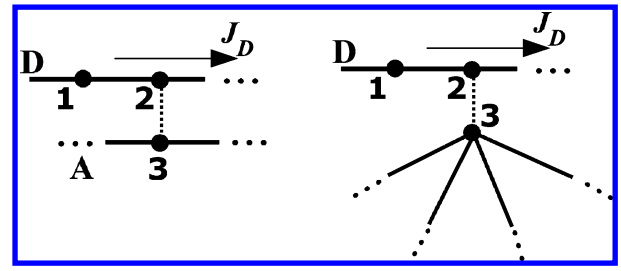

Figure 12. Simple models that demonstrate the origin of band-edge effects in current transfer dynamics. The model on the right is the $n = 4$ analog of the ($n = 2$) model on the left which in turn is a single DA link analog of the model of Figure 3a. The singularity at the band edge is specific to the $n = 2$ case.

$$0 = -i(E_A + 2\Sigma_A(E) - E)\bar{c}_3 - iV_{AD}\bar{c}_2 \quad \text{or}$$

$$\bar{c}_3 = \frac{V_{AD}}{E - E_A - 2\Sigma_A(E)}\bar{c}_2 \qquad (28)$$

and $\Sigma_A(E)$ is given by eq 12 with $K = A$. The factor 2 multiplying $\Sigma_A(E)$ in eq 28 results from the fact that site 3, as part of the infinite A wire, is coupled to two identical seminifinite parts of this wire. Using eq 12 in eq 28 gives

$$\bar{c}_3 = \frac{V_{AD}}{i\Gamma_A(E)}\bar{c}_2 \qquad (29)$$

and from 17 it follows that the current (left or right) out of site 3 is

$$J_{(3\to\text{right})} = \frac{|V_{AD}|^2}{\hbar\Gamma_A(E)}|\bar{c}_2|^2 \qquad (30)$$

This current diverges as $\Gamma_A(E)$ approaches zero at the band edge. It is this singular behavior that manifests itself also in the more complex phenomena described above, but it is important to note that its manifestation is not universal. For example, if wire A is replaced by a system of n identical wires coupled to the driver site 2 via node 3 (Figure 12, right, shows the $n = 4$ case), eq 28 is replaced by $\bar{c}_3 = V_{32}\bar{c}_2(E - E_A - n\Sigma_A(E))^{-1}$. As such, the singularity at the band edge is specific to the $n = 2$ case.

We conclude this section with remarks on this singularity that shed some light on the current transfer formalism and its relationship to scattering theory. The results displayed in Figures 4 and 6−10 give information on different currents in a steady state system with given uniform and unidirectional current flows in the driving wire. It is important to realize that these currents need not satisfy any continuity conditions with respect to the driving current. As such, there is no contradiction in the observation that, under some conditions, a current in wire A that is consistent with a given current in wire D is larger than the latter current. In the equivalent scattering problem, the system is driven by an incoming current in one channel (e.g., the left side of wire D), and the transmitted currents in other channels, together with the reflected current in the original channel (which, by definition, is missing in the present formulation) satisfy the usual continuity relationship that implies current conservation. In the scattering theory analog of the current

transfer problem of Figures 9 and 10, we find[12] that when E_B approaches the band edge from inside the band, the reflection coefficient approaches 1. That is, the net current on wire D becomes essentially zero. The implication for the current transfer calculation, in which the driving current is restricted to remain constant, is that the current in other channels may diverge. While this result is mathematically sound, its physical implication is that moving E_B toward the singularity cannot be accomplished while sustaining a constant current in the driving wire. Consequently, in such situations, the current transfer formalism fails as an approximation to the corresponding scattering theory (see ref 12 for more details).

4. Steady-State Current Transfer in the Density Matrix Formalism: The Effect of Dephasing

In the tight-binding model and in the local site representation, current transfer (the transfer of directional information in the course of a charge transfer process) arises from interferences among different transfer pathways. Therefore at least two interchain links between wires are needed for current transfer to arise. It is therefore of considerable interest to examine the effects of dephasing (decoherence) on the efficiency of these processes. We assume that motion on the driving wire D remains coherent (i.e., a Bloch wave persists), and study the effect of dephasing on the wire B. For this purpose, we recast the steady-state approach to current transfer in the density matrix language and examine the ensuing Liouville space dynamics. In this framework, we can examine relaxation effects, especially the effect of "pure" dephasing (see below), the process that damps nondiagonal elements of the density matrix without affecting the population (diagonal elements) dynamics.

For a closed quantum system described by the time-dependent Schrödinger equation, the transition to a Liouville space description, $i\hbar\, d\hat{\rho}/dt = [\hat{H},\hat{\rho}]$ follows directly. For our tight-binding model in the site representation, the density matrix elements $\rho_{nm} = c_n c_m^*$ are obtained from eq 8

$$d\rho_{nm}/dt = (dc_n/dt)c_m^* + c_n(dc_m^*/dt) \qquad (31)$$

.

Our goal is to extend these equations to steady-state situations involving driving and damping as described above. To this end, we note that eq 9 gives $d\rho_{nm}/dt = 0$ at steady state. Furthermore, population damping enters in the time evolution of diagonal density matrix elements as $d\rho_{nn}/dt = ... - \gamma_n\rho_{nn}$ and in the corresponding equations for nondiagonal elements as $d\rho_{nm}/dt = ... - (1/2)(\gamma_n + \gamma_m)\rho_{nm}$. This remains true also in steady state situations involving infinite wire systems, where apparent damping results from the imaginary part of the self-energy of edge sites (see section 3), i.e. $d\rho_{nm}/dt = 0 = ... - (1/2)(\Gamma_n(E) + \Gamma_m(E))\rho_{nm}$. In addition, pure dephasing is affected by assigning additional damping to the non-diagonal elements of the density matrix (see Appendix A).

The remaining task is then to apply the current driving conditions to these steady-state Liouville equations. We follow the procedure of Segal and Nitzan[13,14] to accomplish this task. In the appendix we outline this procedure for the 2-link version of the model in Figure 3a (see Figure 13). The analysis leads to eqs 32a−34 that provide a solution to the problem by expressing ρ_{ij}, $i,j \in$ D,A, and the associated currents in the D and A wires, $J[n-1\rightarrow n] \equiv 2(\beta_{n,n-1}/\hbar)\, Im\, \hat{\rho}_{n-1,n}$, in terms of properties of the driving current. A generalization of this procedure can be used in more complex situations.[15] It should be noted that this calculation involves an approximation. Since damping of nondiagonal matrix elements is introduced in the site representation and not in the eigenstates basis, it does not correspond to an entirely pure dephasing, that is, the approach induces a small inelastic component in the outgoing electron energy, in the range $\delta E \sim \gamma$ around the injection energy E. Nonetheless, the electron self-energy Σ_K (K = B, A) is evaluated at E. By computing electron transmission with values of $\Sigma_K(E')$ with $E' = E \pm (1/2)\gamma$, we have found that the error associated with this approximation is small for the range of dephasing rates used in the present study.

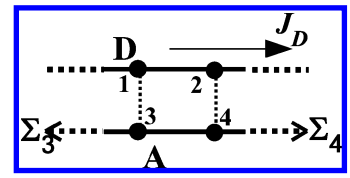

Figure 13. Tight-binding model used to analyze current transfer in the density matrix (Liouville space) formalism.

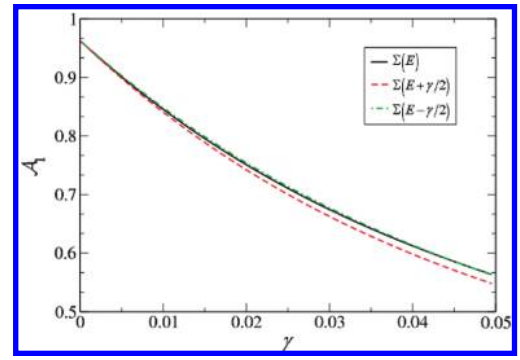

Figure 14. Current asymmetry factor $\mathcal{A}_1$ plotted vs dephasing rate γ for a DA system (Figure 5) characterized by the parameters $N_{DA} = 5$, $E_D = E_A = 0$, $\beta_D = \beta_A = 0.1$, $V_{DA} = 0.01$ and $E = -0.15$. The phase $k_D a = \arccos((E - E_D)/2\beta_D)$ was taken positive, implying leftward driving current. Also shown are results obtained from using $\Sigma_A(E + \gamma/2)$ (dashed line, red) and $\Sigma_A(E - \gamma/2)$ (dash-dotted line, green), instead of $\Sigma_A(E)$ in this calculation.

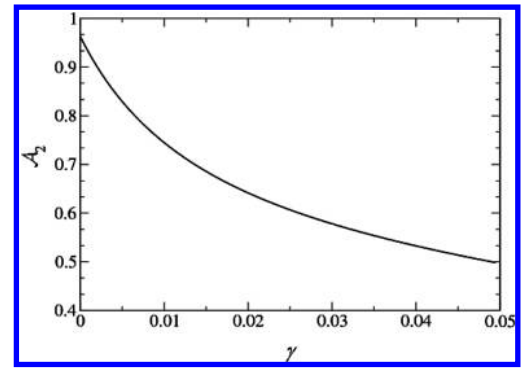

Figure 15. Current asymmetry factor $\mathcal{A}_2$ plotted vs the dephasing rate γ for a DBA system (Figure 5) characterized by the parameters $N_{DB} = 5$, $N_B = 3$, $N_{BA} = 1$, $E_D = E_B = E_A = 0$, $\beta_D = \beta_B = \beta_A = 0.1$, $V_{DB} = V_{BA} = 0.01$.

We next describe examples that show the effect of dephasing, introduced as described above, on current transfer. In these calculations we have assigned dephasing rates γ to the N_{DA} sites on the A wire that are linked to the D wire in the DA system and to the $N_{DB} + N_B + N_{BA}$ sites on the B wire that connect between the D and A wires in the DBA system (Figure 5). Results are shown in Figures 14 and 15, respectively. Interestingly, while the current transfer efficiency drops with increasing γ, the effect persists up to relatively large values of the dephasing rate, of the order of the other tight binding energy parameters in the system. A similar observation was made in the time domain study of ref 1.

5. Conclusions

We use the term current transfer to describe a combined process of charge and momentum transfer. Within the tight-binding models used here, current transfer is described as a coherent phenomenon resulting from the interference among transition and/or tunneling paths. We have investigated the dependence of this phenomenon on several key systems parameters focusing on two simple models. One focuses on charge transfer in two wires (donor and acceptor, or driving and driven wires) and the other has a bridge wire between these donor and acceptor.

This study advances a steady-state theory of current transfer, complementing a previous analysis in the time domain. On the experimental side, the present analysis corresponds to the analogue of the optical experiments in refs 2 and 3 if illumination were continuous. Another possible realization of the models presented here would be to attach a ring shaped molecule to a current carrying molecular wire, mimicking a setup similar to the model in Figure 3c, but without the A site. In such a setup, the current in the linear wire would drive a circular current in the ring (the reverse of the operation described in the discussion of Figure 3c), which may perhaps be detected by its magnetic field.[16]

The current transfer theory presented here is based on an independent electron model. Electron−electron interactions can lead to current transfer phenomena also in diffusive transport.[17] Such interactions are believed to dominate charge fractionalization in the momentum conserving current transfer observed between parallel mesoscopic wires by Steinberg et al.[18] In our analysis, current transfer originates from interference between different transmission or tunneling paths. Such interference phenomena in molecular wires and nanodots have received considerable recent attention[19−25] We have also formulated the current transfer theory in the density matrix representation, emphasizing the difference between the resulting steady-state equations and those that could be inferred from using the Liouville equation. This density matrix formulation enables investigations of decoherence effects on the current transfer phenomenon, demonstrating the expected reduction in current transfer efficiency in the presence of dephasing.

The current transfer models considered here are formulated in terms of quantum dynamical equations with well-defined "driving boundary conditions". Such boundary conditions differ from the more familiar scattering boundary conditions. In the scattering case, the wave function in the D wire consists of incoming and scattering components, with the latter containing reflected and transmitted parts. In contrast, in the driving problem considered here, the D wire is restricted to carry a steady Bloch-wave function, imposed by an external driving condition (e.g., the continuous wave analogs of the experiments of refs 4, and 2, 3 as discussed above), that is assumed to be insensitive to the dynamical processes in the rest of the system. The relationship between the two problems will be considered elsewhere.[12]

Acknowledgment. V.BM. thanks the Israel Minisry of Science for a fellowship received under the program for Progressing Women in Science. The research of A.N. is supported by the European Science Council (FP7/ERC Grant No. 226628), the German-Israel Foundation, the Israel−Niedersachsen Research Fund, the U.S.−Israel binational Science Foundation and the Israel Science Foundation. The research of S.S.S is supported by the University of Cyprus. D.N.B. thanks the U.S. National Science Foundation for support (CHE-0718043).

Appendix

Here we implement the driving conditions described in sections 1 and 2 in the steady-state Liouville eq 31 for the model of Figure 13, following the procedure of Segal and Nitzan.[13,14] Using eq 31 with eqs 8 and 9 (supplemented by the self-energy terms imposed on site 3 and 4 that are taken as edge sites of wire A) leads to the steady state equations

$$\begin{pmatrix} -i\Gamma_3 & 0 & -\beta_A & \beta_A \\ 0 & -i\Gamma_4 & \beta_A & -\beta_A \\ -\beta_A & \beta_A & -(i/2)(\Gamma_3+\Gamma_4)+\tilde{E}_{34} & 0 \\ \beta_A & -\beta_A & 0 & -(i/2)(\Gamma_3+\Gamma_4)+\tilde{E}_{43} \end{pmatrix} \begin{pmatrix} \rho_{33} \\ \rho_{44} \\ \rho_{34} \\ \rho_{43} \end{pmatrix} = V \begin{pmatrix} \rho_{31}-\rho_{13} \\ \rho_{42}-\rho_{24} \\ \rho_{32}-\rho_{14} \\ \rho_{23}-\rho_{41} \end{pmatrix} \tag{32a}$$

where $\tilde{E}_{nm} = \tilde{E}_n - \tilde{E}_m$, $\Sigma_n(E) = \Lambda_n(E) - (i/2)\Gamma_n(E)$, and $\tilde{E}_n = E_n + \Lambda_n(E)$. As before, we take $E_3 = E_4 \equiv E_A$ and $\Sigma_3(E) = \Sigma_4(E) \equiv \Sigma_A(E)$; however, we retain the specific site designations here for ease of presentation. Equation 32a is the standard steady-state Liouville equation for the density matrix elements of the A wire, and shows explicitly their dependence on density matrix elements that mix A and D sites. For the latter, we again employ again eqs 8, 9, and 31 supplemented by the self-energy contributions. We find

$$\begin{pmatrix} E-\tilde{E}_3-(i/2)\Gamma_3 & 0 & 0 & -\beta_A \\ 0 & E-\tilde{E}_4-(i/2)\Gamma_4 & -\beta_A & 0 \\ 0 & -\beta_A & E-\tilde{E}_3-(i/2)\Gamma_3 & 0 \\ -\beta_A & 0 & 0 & E-\tilde{E}_4-(i/2)\Gamma_4 \end{pmatrix} \begin{pmatrix} \rho_{13} \\ \rho_{24} \\ \rho_{23} \\ \rho_{14} \end{pmatrix} = V \begin{pmatrix} \rho_{11} \\ \rho_{22} \\ \rho_{21} \\ \rho_{12} \end{pmatrix} \tag{33a}$$

Equation 33a describes the mixed DA density matrix elements, $\rho_{nm} = \rho^*_{mn}$, $n \in D$, $m \in A$, in terms of elements associated with the D wire only. As noted in ref 13, these equations deviate from the standard Liouville equations. In evaluating eq 31, the time derivatives associated with the driver coefficients are taken as $\hbar\, dc_n/dt = -iEc_n$, $n = 1,2$ (which expresses the driving condition), rather then being derived from the system Hamiltonian. Further information about the driving enters through the explicit identification of $\rho_{nm} = c_n c^*_m$ for $n,m \in D$ which implies that

$$\rho_{22} = \rho_{11}; \quad \rho_{21} = \rho_{12}^{*} = \mathrm{e}^{ik_{\mathrm{D}}a}\rho_{11} \tag{34}$$

The effect of pure dephasing may now be included in this dynamics using the standard phenomenological approach in which additional damping is assigned to nondiagonal elements of the density matrix: $\mathrm{d}\rho_{ij}/\mathrm{d}t = -\gamma_{ij}\rho_{ij}$. In the calculations below we assume that different local levels are affected independently by the thermal environment, whereupon $\gamma_{ij} = (1/2)(\gamma_i + \gamma_j)$, and we furthermore take $\gamma_j = \gamma$ for all levels on the A and B wires (when applicable). Also, by definition, the driving dynamics is assumed unaffected by the thermal environment. This implies that zero dephasing should be assigned to levels in the D wire, i.e., $\gamma_j = 0$ for $j \in D$. Equations 32a and 33a become

$$\begin{pmatrix} -i\Gamma_3 & 0 & -\beta_{\mathrm{A}} & \beta_{\mathrm{A}} \\ 0 & -i\Gamma_4 & \beta_{\mathrm{A}} & -\beta_{\mathrm{A}} \\ -\beta_{\mathrm{A}} & \beta_{\mathrm{A}} & -(i/2)(\Gamma_3 + \Gamma_4 + 2\gamma) + \tilde{E}_{34} & 0 \\ \beta_{\mathrm{A}} & -\beta_{\mathrm{A}} & 0 & -(i/2)(\Gamma_3 + \Gamma_4 + 2\gamma) + \tilde{E}_{43} \end{pmatrix} \begin{pmatrix} \rho_{33} \\ \rho_{44} \\ \rho_{34} \\ \rho_{43} \end{pmatrix} = V \begin{pmatrix} \rho_{31} - \rho_{13} \\ \rho_{42} - \rho_{24} \\ \rho_{32} - \rho_{14} \\ \rho_{23} - \rho_{41} \end{pmatrix} \tag{32b}$$

$$\begin{pmatrix} E - \tilde{E}_3 - \frac{i}{2}(\Gamma_3 + \gamma) & 0 & 0 & -\beta_{\mathrm{A}} \\ 0 & E - \tilde{E}_4 - \frac{i}{2}(\Gamma_4 + \gamma) & -\beta_{\mathrm{A}} & 0 \\ 0 & -\beta_{\mathrm{A}} & E - \tilde{E}_3 - \frac{i}{2}(\Gamma_3 + \gamma) & 0 \\ -\beta_{\mathrm{A}} & 0 & 0 & E - \tilde{E}_4 - \frac{i}{2}(\Gamma_4 + \gamma) \end{pmatrix} \begin{pmatrix} \rho_{13} \\ \rho_{24} \\ \rho_{23} \\ \rho_{14} \end{pmatrix} = V \begin{pmatrix} \rho_{11} \\ \rho_{22} \\ \rho_{21} \\ \rho_{12} \end{pmatrix} \tag{33b}$$

Finally, the solutions to eq 33a

$$\rho_{13} = \frac{\rho_{11} + \beta_{\mathrm{A}}\rho_{12}}{X_3 + \beta_{\mathrm{A}}{}^2/X_4}; \quad \rho_{23} = \frac{\rho_{21} + \beta_{\mathrm{A}}\rho_{22}}{X_3 + \beta_{\mathrm{A}}{}^2/X_4} \tag{35}$$

where $X_n = E - \tilde{E}_n - (i/2)\Gamma_n$, $n \in A$, satisfy

$$\frac{\rho_{13}}{\rho_{23}} = \frac{\rho_{11} + \beta_{\mathrm{A}}\rho_{12}}{\rho_{21} + \beta_{\mathrm{A}}\rho_{22}} = \mathrm{e}^{-ik_{\mathrm{D}}a} \tag{36}$$

This clearly remains true also for eq 33b, where Γ_n is replaced by $\Gamma_n + \gamma$. In systems with more interconnnections between the D and A wires we find similarly

$$\frac{\rho_{j'n}}{\rho_{jn}} = \mathrm{e}^{-ik_D(j-j')a}; \qquad n \in A; \quad j,j' \in D \tag{37}$$

That is, these ratios behave as if $\rho_{jn} = c_j c_n^{*}$ also in the general case involving damping. These relationships can be used, in more complex models, to reduce the number of equations that needs to be solved, i.e., the size of the matrices that need to be inverted.

References and Notes

(1) Skourtis, S. S.; Beratan, D. N.; Naaman, R.; Nitzan, A.; Waldeck, D. H. *Phys. Rev. Lett.* **2008**, *101*, 238103.
(2) Ray, K.; Ananthavel, S. P.; Waldeck, D. H.; Naaman, R. *Science* **1999**, *283*, 814.
(3) Wei, J. J.; Schafmeister, C.; Bird, G.; Paul, A.; Naaman, R.; Waldeck, D. H. *J. Phys. Chem. B* **2006**, *110*, 1301.
(4) Güdde, J.; Rohleder, M.; Meier, T.; Koch, S. W.; Höfer, U. *Science* **2007**, *318*, 1287.
(5) Barth, I.; Manz, J.; Shigeta, Y.; Yagi, K. *J. Am. Chem. Soc.* **2006**, *128*, 7043.
(6) Barth, I.; Manz, J. *Angew. Chem., Int. Ed.* **2006**, *45*, 2962.
(7) Barth, I.; Manz, J.; Serrano-Andres, L. *Chem. Phys.* **2008**, *347*, 263.
(8) Nobusada, K.; Yabana, K. *Phys. Rev. A* **2007**, *75*, 032518.
(9) Lin, L.-L.; Leng, J.-C.; Song, X.-N.; Li, Z.-L.; Luo, Y.; Wang, C.-K. *J. Phys. Chem. C* **2009**, *113*, 14474.
(10) Aviram, A. *J. Am. Chem. Soc.* **1988**, *110*, 5687.
(11) Skourtis, S. S.; Beratan, D. N. *Adv. Chem. Phys.* **1999**, *106*, 377.
(12) Ben-Moshe, V.; Nitzan, A.; Skourtis, S. S. **2010**, to be published.
(13) Segal, D.; Nitzan, A. *Chem. Phys.* **2001**, *268*, 315.
(14) Segal, D.; Nitzan, A. *Chem. Phys.* **2002**, *281*, 235.
(15) Ben-Moshe, V. Thesis, Tel Aviv University, 2009.
(16) Ernzerhof, M.; Bahmann, H.; Goyer, F.; Zhuang, M.; Rocheleau, P. *J. Chem. Theory Comput.* **2006**, *2*, 1291.
(17) Raikh, M. E.; von Oppen, F. *Phys. Rev. Lett.* **2002**, *89*, 106601.
(18) Steinberg, H.; Barak, G.; Yacoby, A.; Pfeiffer, L. N.; West, K. W.; Halperin, B. I.; Le Hur, K. *Nat. Phys.* **2008**, *4*, 116.
(19) Solomon, G. C.; Andrews, D. Q.; Hansen, T.; Goldsmith, R. H.; Wasielewski, M. R.; Duyne, R. P. V.; Ratner, M. A. *J. Chem. Phys.* **2008**, *129*, 054701.
(20) Andrews, D. Q.; Solomon, G. C.; Goldsmith, R. H.; Hansen, T.; Wasielewski, M. R.; Duyne, R. P. V.; Ratner, M. A. *J. Phys. Chem. C* **2008**.
(21) Ke, S. H.; Yang, W. T.; Baranger, H. U. *Nano Lett.* **2008**, *8*, 3257.
(22) Begemann, G.; Darau, D.; Donarini, A.; Grifoni, M. *Phys. Rev. B (Condens. Matter Mater. Phys.)* **2008**, *77*, 201406.
(23) Donarini, A.; Begemann, G.; Grifoni, M. *Nano Lett.* **2009**, *9*, 2897.
(24) Xiao, D. Q.; Skourtis, S. S.; Rubtsov, I. V.; Beratan, D. N. *Nano Lett.* **2009**, *9*, 1818.
(25) Beratan, D. N.; Skourtis, S. S.; Balabin, I. A.; Balaeff, A.; Keinan, S.; Venkatramani, R.; Xiao, D. *Acc. Chem. Res.* **2009**, *42*, 1669.

JP100661F